Aalborg Universitet

Standard SOGI-FLL and Its Close Variants

Precise Modeling in LTP Framework and Determining Stability Region/Robustness Metrics

Golestan, Saeed; Guerrero, Josep M.; Vasquez, Juan C.; Abusorrah, Abdullah M.; Al-Turki, Yusuf

Standard SOGI-FLL and Its Close Variants: Precise LTP Modeling and Determining Stability Region/Robustness Metrics

Saeed Golestan, *Senior Member, IEEE*, Josep M. Guerrero, *Fellow, IEEE*, Juan. C. Vasquez, *Senior Member, IEEE*, Abdullah M. Abusorrah, *Senior Member, IEEE*, and Yusuf Al-Turki, *Senior Member, IEEE*

Abstract—In recent years, single-phase frequency-locked loops (FLLs) are gaining more popularity as a signal processing and synchronization tool in a wide variety of engineering applications. In the power and energy area, a basic structure in designing the majority of available single-phase FLLs is the second-order generalized integrator-based FLL (SOGI-FLL), which is a nonlinear feedback control system. This nonlinearity makes the SOGI-FLL analysis complicated. To deal with this problem, some attempts to derive linear models for the SOGI-FLL have been made in very recent years. The available linear models, however, are not able to accurately predict the dynamic behavior, stability region, and robustness metrics of the SOGI-FLL. The situation is even worse for close variants of the SOGI-FLL because some of them have no linear model at all. Filling these gaps in research is the main goal of this paper. To this end, the structural relationship among the SOGI-FLL and its variants is identified first. Based on this information and deriving the LTP model of a recently proposed extended SOGI-FLL, the LTP models of the standard SOGI-FLL and its close variants are obtained. The accuracy assessment of these LTP models, discussion about their limitations, and performing the stability analysis using them are other contributions of this paper.

Index Terms—All-pass filter (APF), enhanced phase-locked loop (EPLL), frequency-locked loop (FLL), linear Kalman filter (LKF), linear time-invariant (LTI), linear time-periodic (LTP), modeling, second-order generalized integrator (SOGI), single-phase systems, synchronization.

I. INTRODUCTION

SINGLE-PHASE frequency-locked loops (FLLs) are often known as a tool for the grid synchronization of power converters [1]. It is, however, not their only important role. They are now more and more employed as a tool for signal processing, monitoring, and control in different engineering applications [2]–[7].

In the power and energy area, a quite large number of single-phase FLLs exist. Most of these FLLs, however, are based
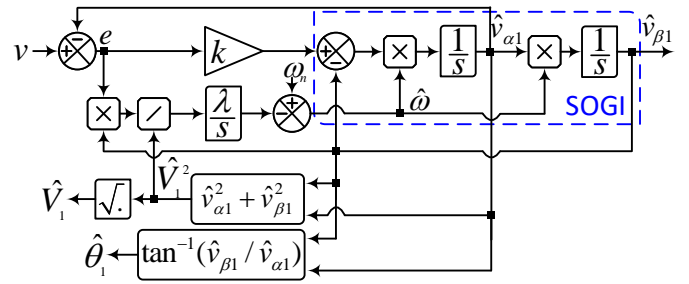
Fig. 1. Block diagram representation of SOGI-FLL. k and λ are the design parameters of the SOGI-FLL. v is the single-phase input signal, $\hat{v}_{\alpha 1}$ is an estimation of the fundamental component of this signal, and $\hat{v}_{\beta 1}$ is an estimation of its quadrature version. ω_n is the nominal angular frequency of the single-phase input signal, and $\hat{\omega}$, $\hat{V}_1$, and $\hat{\theta}_1$ are estimations of the angular frequency, amplitude, and phase angle of its fundamental component, respectively.

on a basic structure, which is known as the SOGI-FLL. The block diagram of the SOGI-FLL can be observed in Fig. 1 [1], [7].[1] Here, the SOGI is an adaptive resonant controller with a pair of complex-conjugate poles at the fundamental frequency. According to the internal model principle, including the SOGI in a unity feedback control loop, as shown in Fig. 1, provides an estimation of the fundamental component of the single-phase input signal and its $90°$ phase-shifted version. The center frequency of the SOGI is adapted to frequency changes using a frequency estimator. The governing differential equation of this estimator can be obtained using the gradient descent method [1], [7], [8].

In recent years, extensive studies on the SOGI-FLL structure have been conducted in the literature. Gaining a deeper insight into the SOGI-FLL performance, improving its dynamic behavior and/or filtering capability in the presence of grid voltage disturbances, and achieving a more robust performance at low sampling frequencies and/or in fixed-point implementations are the main objectives of these studies [7]. In what follows, a brief review of some of these studies is presented.

It is discussed in [7], [9], [10] that using the discretization methods such as the backward/forward Euler and the third-order Adams–Bashforth method results in noticeable numerical errors in the digital implementation of the SOGI-FLL
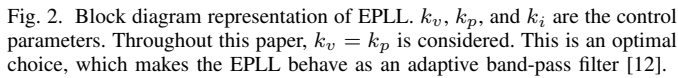
---

[1]The original structure of the SOGI-FLL in [1] includes a feedback loop that multiples the input signal of the integrator of its frequency estimator by the estimated frequency $\hat{\omega}$. This multiplication is neglected in this paper.

Fig. 2. Block diagram representation of EPLL. k_v, k_p, and k_i are the control parameters. Throughout this paper, $k_v = k_p$ is considered. This is an optimal choice, which makes the EPLL behave as an adaptive band-pass filter [12].

Fig. 4. Block diagram representation of SSLKF-FLL. k_α, k_β, and λ are the control gains.

Fig. 3. Block diagram representation of APF-FLL.

Fig. 5. Block diagram representation of eSOGI-FLL. k, k', λ, and λ' are the control gains.

Fig. 6. Block diagram representation of SOGI-FLL-WPF. k_1, k_2, and λ are the control gains.

when the sampling frequency is low. A possible approach to deal with this challenge is designing a discrete-time FLL by considering an exact discrete model of a single-phase signal generator [11]. An alternative method is using the enhanced PLL (EPLL) concept [12], [13]. The EPLL, which is mathematically equivalent to the SOGI-FLL under certain conditions [7], [12], offers high robustness at low sampling frequencies without any requirement for the inverse tangent and square root calculation. The block diagram representation of the EPLL can be observed in Fig. 2.

By obtaining the transfer functions between the output signals $\hat{v}_{\alpha1}$ and $\hat{v}_{\beta1}$ and the input signal v in the SOGI-FLL[2], it is shown in [14] that the SOGI-FLL provides a more harmonic filtering and a less sub-harmonic/dc filtering capability in its β-axis output compared to the α-axis one. To provide the same level of the disturbance rejection capability in these outputs, replacing one integrator of the SOGI with a first-order all-pass filter (APF) is proposed in [14]. Fig. 3 illustrates the resultant structure, which is referred to as the APF-FLL here.[3]

Instead of using a SOGI in the unity feedback loop, employing a linear Kalman filter (LKF) for extracting the fundamental component of the single-phase input signal and its quadrature version is proposed in [15]. A frequency estimator similar to that of the SOGI-FLL is used for adapting the LKF to frequency changes. The gains of LKF are updated in each sampling period, according to the Kalman filter theory. This structure is called the LKF-FLL in [15]. In [16], it is demonstrated that there is no noticeable performance differ-

ence between the LKF-FLL and its steady-state version [called the steady-state LKF-FLL (SSLKF-FLL)] in grid applications as the grid frequency and, therefore, the Kalman gains of the LKF-FLL have small variations around their nominal value in the steady state. The block diagram representation of the SSLKF-FLL in the continuous-time domain can be observed in Fig. 4.

To obtain a theoretically limitless speed in the extraction of the fundamental component of a single-phase input signal and its quadrature version, adding a degree of freedom to a standard SOGI is proposed in [17]. It is also recommended in [17] to use both the in-phase and quadrature-phase signals of the fundamental component in the detection of the grid frequency. Fig. 5 shows the resulting structure, which is referred to as

---

[2]To obtain these transfer functions, we have to assume that the estimated angular frequency $\hat{\omega}$ is a constant.

[3]To improve the filtering capability of the APF-FLL, passing its $\alpha\beta$ output signals through two complex band-pass filters are proposed in [14]. These complex filters are not considered in this paper.

the extended SOGI-FLL (eSOGI-FLL) here.[4] Designing and including rate limitation and sign-correct anti-windup strategy into the frequency estimator are other contributions of [17], which are not considered in this paper.

To make the SOGI-FLL immune to the grid voltage dc component and improve its harmonic/interharmonic filtering capability, including a prefilter before the SOGI-FLL input is proposed in [18]. Fig. 6 illustrates the block diagram of the resulting structure, which is referred to as the SOGI-FLL with prefilter (SOGI-FLL-WPF). Notice that the prefilter is an adaptive band-pass filter centered at the fundamental frequency, which is implemented by using a SOGI in a unity feedback loop. Notice also that the prefilter is adapted to frequency changes using a frequency feedback loop.

The SOGI-FLL, EPLL, APF-FLL, SSLKF-FLL, eSOGI-FLL, and SOGI-FLL-WPF are all nonlinear feedback control systems. This non-linearity makes their analysis a nontrivial task. A solution to deal with this challenge is providing linear models for them. For the APF-FLL, SSLKF-FLL, and eSOGI-FLL, no linear model has yet been presented. For the SOGI-FLL, EPLL, and SOGI-FLL-WPF, however, some attempts have been made in very recent years. In [19], for example, some linear time-invariant (LTI) models for the SOGI-FLL and SOGI-FLL-WPF are presented. These LTI models can predict the average dynamic behavior of the SOGI-FLL and SOGI-FLL-WPF. However, they cannot predict the double-frequency damped oscillations (which inherently exist in the transient response of the SOGI-FLL and SOGI-FLL-WPF) and the coupling between their phase and amplitude estimation dynamics. This fact can be clearly observed in Figs. 6-8 in [19]. In [20], deriving linear time-periodic (LTP) models for the SOGI-FLL and EPLL are discussed. Compared to the LTI models, the derived LTP models provide higher accuracy in predicting the phase/frequency estimation dynamics of the SOGI-FLL and EPLL. However, they still suffer from some inaccuracies because they neglect the grid voltage amplitude variations and the dynamic coupling between the phase and amplitude variables in the SOGI-FLL and EPLL.

The main aim of this paper, which is an extension of the work in [20], is to present precise LTP models for the SOGI-FLL, EPLL, APF-FLL, SSLKF-FLL, eSOGI-FLL, and SOGI-FLL-WPF. This modeling is an important contribution to the field mainly because it facilitates the analysis of these FLL/PLL structures. To demonstrate this fact, a thorough analysis of the SOGI-FLL using its new LTP model is conducted.

II. LTP MODELING

A. Relationship Between Synchronization Systems

If we assume that the estimated frequency $\hat{\omega}$ is a constant, the characteristic transfer functions of the SOGI-FLL [Fig. 1], APF-FLL [Fig. 3], SSLKF-FLL [Fig. 4], and eSOGI-FLL [Fig. 5] can be obtained as expressed in Table I. Based on these transfer functions and considering the fact that the frequency estimator of the eSOGI-FLL has an additional degree of

---

TABLE I
CHARACTERISTIC TRANSFER FUNCTIONS

	$G_\alpha(s) = \frac{\hat{v}_{\alpha 1}(s)}{v(s)}$	$G_\beta(s) = \frac{\hat{v}_{\beta 1}(s)}{v(s)}$
SOGI-FLL	$\dfrac{k\hat{\omega}s}{s^2 + k\hat{\omega}s + \hat{\omega}^2}$	$\dfrac{k\hat{\omega}^2}{s^2 + k\hat{\omega}s + \hat{\omega}^2}$
APF-FLL	$\dfrac{k\hat{\omega}^2 + k\hat{\omega}s}{s^2 + k\hat{\omega}s + \hat{\omega}^2 + k\hat{\omega}^2}$	$\dfrac{k\hat{\omega}^2 - k\hat{\omega}s}{s^2 + k\hat{\omega}s + \hat{\omega}^2 + k\hat{\omega}^2}$
SSLKF-FLL	$\dfrac{k_\alpha s - k_\beta \hat{\omega}}{s^2 + k_\alpha s + \hat{\omega}^2 - k_\beta \hat{\omega}}$	$\dfrac{k_\beta s + k_\alpha \hat{\omega}}{s^2 + k_\alpha s + \hat{\omega}^2 - k_\beta \hat{\omega}}$
eSOGI-FLL	$\dfrac{k\hat{\omega}s - k'\hat{\omega}^2}{s^2 + k\hat{\omega}s + \hat{\omega}^2 - k'\hat{\omega}^2}$	$\dfrac{k'\hat{\omega}s + k\hat{\omega}^2}{s^2 + k\hat{\omega}s + \hat{\omega}^2 - k'\hat{\omega}^2}$

---

freedom (the control gain λ') compared to that of the SOGI-FLL, APF-FLL, and SSLKF-FLL, the following conclusions can be made.

- The SOGI-FLL is a special case of the eSOGI-FLL, where $k' = 0$ and $\lambda' = 0$.
- The APF-FLL is a special case of the eSOGI-FLL, where $k' = -k$ and $\lambda' = 0$.
- The SSLKF-FLL is a special case of the eSOGI-FLL, where $k\hat{\omega} = k_\alpha$, $k'\hat{\omega} = k_\beta$, and $\lambda' = 0$.[5]

The above observations suggest that the LTP modeling of only the eSOGI-FLL suffices for obtaining the LTP models of the SOGI-FLL, EPLL, APF-FLL, SSLKF-FLL, and SOGI-FLL-WPF. Notice that the EPLL is mathematically equivalent to the SOGI-FLL [12]. Therefore, the LTP model of the EPLL will be the same as that of the SOGI-FLL. Notice also that the LTP model of the SOGI-FLL-WPF can be directly obtained using the LTP model of the SOGI-FLL. These facts will be discussed with more details later.

B. LTP Modeling of eSOGI-FLL

1) Assumptions and Definitions: During the modeling procedure, the presence of disturbance components in the single-phase input signal is neglected, and the single-phase input signal is considered as

$$v(t) = V_1 \cos(\theta_1) \tag{1}$$

where V_1 and $\theta_1 = \int \omega dt$ are the amplitude and phase angle of the fundamental component of the input signal v, respectively, and ω is the fundamental angular frequency.

From Fig. 7, which shows the Bode plot of the characteristic transfer functions of the eSOGI-FLL for different values of control parameters, it can be observed that both transfer functions G_α and G_β have a unity gain (0 dB gain) at the fundamental frequency. It is also observed that G_α and G_β have respectively a zero phase and $-90°$ phase at the fundamental frequency. These imply that the signal $\hat{v}_{\alpha 1}$ in the eSOGI-FLL structure is an estimation of the fundamental component of the input signal v, and the signal $\hat{v}_{\beta 1}$ is its $90°$ phase-shifted version. Considering this fact, the output signals $\hat{v}_{\alpha 1}$ and $\hat{v}_{\beta 1}$ can be considered as

$$\hat{v}_{\alpha 1}(t) = \hat{V}_1 \cos(\hat{\theta}_1), \quad \hat{v}_{\beta 1}(t) = \hat{V}_1 \sin(\hat{\theta}_1) \tag{2}$$

---

[4]It is called the modified SOGI-FLL in [17]. However, to avoid confusion with some other SOGI-based structures with the same name, it is referred to as the eSOGI-FLL here.

[5]As k_α and k_β are constants, $k_\alpha = k\omega_n$ and $k_\beta = k'\omega_n$ need to be considered in practice.
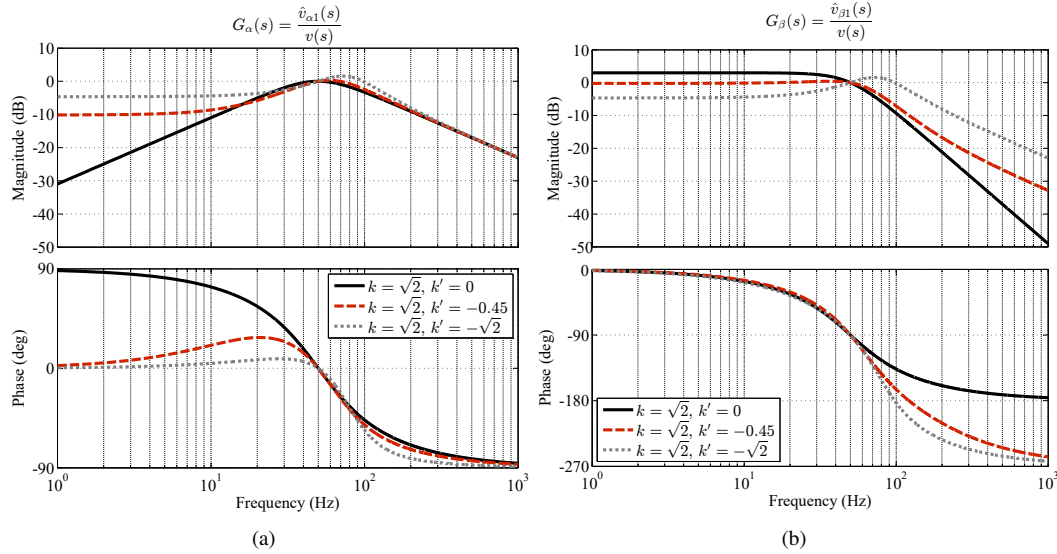
Fig. 7. Frequency response of the characteristic transfer functions of the eSOGI-FLL. (a) Frequency response of $G_\alpha(s) = \hat{v}_{\alpha1}(s)/v(s)$. (b) Frequency response of $G_\beta(s) = \hat{v}_{\beta1}(s)/v(s)$. The characteristic transfer functions of the eSOGI-FLL can be found in Table I. In obtaining these Bode plots, $\hat{\omega} = \omega_n = 2\pi50$ rad/s is considered.

where $\hat{V}_1$ and $\hat{\theta}_1$ are estimations of V_1 and θ_1 in (1), respectively.

The eSOGI-FLL is also assumed to be working in a quasi-locked state, which is corresponding to consider $\hat{V}_1 \approx V$, $\hat{\omega} \approx \omega$, and $\hat{\theta}_1 \approx \theta_1$.

We also define the actual and estimated parameters as a nominal value plus a small perturbation, as expressed in (3).

$$
\begin{aligned}
V_1 &= V_n + \Delta V_1, & \hat{V}_1 &= V_n + \Delta \hat{V}_1 \\
\omega &= \omega_n + \Delta\omega, & \hat{\omega} &= \omega_n + \Delta\hat{\omega} \\
\theta_1 &= \theta_n + \Delta\theta_1, & \hat{\theta}_1 &= \theta_n + \Delta\hat{\theta}_1
\end{aligned}
\tag{3}
$$

In (3), Δ and the subscript n denote a small perturbation and a nominal value, respectively. Throughout this paper, $V_n = 1$ p.u., $\omega_n = 2\pi50$ rad/s, and $\theta_n = \int \omega_n dt = \omega_n t$ are considered.

2) Governing Differential Equations: According to Fig. 5, the estimated angular frequency, phase angle, and amplitude by the eSOGI-FLL can be expressed as

$$
\hat{\omega} = \omega_n + \int \frac{(v - \hat{v}_{\alpha1})(\lambda'\hat{v}_{\alpha1} - \lambda\hat{v}_{\beta1})}{\hat{V}_1^2} dt
\tag{4a}
$$

$$
\hat{\theta}_1 = \tan(\hat{v}_{\beta1}/\hat{v}_{\alpha1})
\tag{4b}
$$

$$
\hat{V}_1 = \sqrt{\hat{v}_{\alpha1}^2 + \hat{v}_{\beta1}^2}.
\tag{4c}
$$

Differentiation from (4) with respect to time results in

$$
\frac{d\hat{\omega}}{dt} = \frac{\lambda'(v - \hat{v}_{\alpha1})\hat{v}_{\alpha1} - \lambda(v - \hat{v}_{\alpha1})\hat{v}_{\beta1}}{\hat{V}_1^2}
\tag{5a}
$$

$$
\frac{d\hat{\theta}_1}{dt} = \frac{\hat{v}_{\alpha1}\frac{d\hat{v}_{\beta1}}{dt} - \hat{v}_{\beta1}\frac{d\hat{v}_{\alpha1}}{dt}}{\hat{v}_{\alpha1}^2 + \hat{v}_{\beta1}^2} = \frac{\hat{v}_{\alpha1}\frac{d\hat{v}_{\beta1}}{dt} - \hat{v}_{\beta1}\frac{d\hat{v}_{\alpha1}}{dt}}{\hat{V}_1^2}
\tag{5b}
$$

$$
\frac{d\hat{V}_1}{dt} = \frac{\hat{v}_{\alpha1}\frac{d\hat{v}_{\alpha1}}{dt} + \hat{v}_{\beta1}\frac{d\hat{v}_{\beta1}}{dt}}{\hat{V}_1}
\tag{5c}
$$

where the time derivatives $\frac{d\hat{v}_{\alpha1}}{dt}$ and $\frac{d\hat{v}_{\beta1}}{dt}$, according to Fig. 5, are equal to

$$
\frac{d\hat{v}_{\alpha1}}{dt} = -\hat{\omega}\hat{v}_{\beta1} + k\hat{\omega}(v - \hat{v}_{\alpha1})
\tag{6a}
$$

$$
\frac{d\hat{v}_{\beta1}}{dt} = +\hat{\omega}\hat{v}_{\alpha1} + k'\hat{\omega}(v - \hat{v}_{\alpha1}).
\tag{6b}
$$

Substituting (6) into (5) gives

$$
\frac{d\hat{\omega}}{dt} = \frac{\lambda'(v - \hat{v}_{\alpha1})\hat{v}_{\alpha1} - \lambda(v - \hat{v}_{\alpha1})\hat{v}_{\beta1}}{\hat{V}_1^2}
\tag{7a}
$$

$$
\frac{d\hat{\theta}_1}{dt} = \hat{\omega} + \frac{k'\hat{\omega}(v - \hat{v}_{\alpha1})\hat{v}_{\alpha1} - k\hat{\omega}(v - \hat{v}_{\alpha1})\hat{v}_{\beta1}}{\hat{V}_1^2}
\tag{7b}
$$

$$
\frac{d\hat{V}_1}{dt} = \frac{k\hat{\omega}(v - \hat{v}_{\alpha1})\hat{v}_{\alpha1} + k'\hat{\omega}(v - \hat{v}_{\alpha1})\hat{v}_{\beta1}}{\hat{V}_1}.
\tag{7c}
$$

Equations (7) are the governing differential equations of the eSOGI-FLL, which are nonlinear. Therefore, they need to be linearized for obtaining a linear model for the eSOGI-FLL.

3) Linearization: Two main nonlinear terms of the differential equations (7) are $\frac{1}{\hat{V}_1}(v - \hat{v}_{\alpha1})\hat{v}_{\alpha1}$ and $\frac{1}{\hat{V}_1}(v - \hat{v}_{\alpha1})\hat{v}_{\beta1}$, which are linearized in what follows.

Substituting (1) and (2) into the above nonlinear terms results in

$$
\frac{1}{\hat{V}_1}(v - \hat{v}_{\alpha1})\hat{v}_{\alpha1} = \left(V_1\cos(\theta_1) - \hat{V}_1\cos(\hat{\theta}_1)\right)\cos(\hat{\theta}_1)
$$
$$
= \frac{1}{2}\left[V_1\cos(\theta_1 - \hat{\theta}_1) + V_1\cos(\theta_1 + \hat{\theta}_1) - \hat{V}_1 - \hat{V}_1\cos(2\hat{\theta}_1)\right]
\tag{8a}
$$

$$
\frac{1}{\hat{V}_1}(v - \hat{v}_{\alpha1})\hat{v}_{\beta1} = \left(V_1\cos(\theta_1) - \hat{V}_1\cos(\hat{\theta}_1)\right)\sin(\hat{\theta}_1)
$$
$$
= \frac{1}{2}\left[-V_1\sin(\theta_1 - \hat{\theta}_1) + V_1\sin(\theta_1 + \hat{\theta}_1) - \hat{V}_1\sin(2\hat{\theta}_1)\right].
\tag{8b}
$$

Considering the definitions (3), (8) can be rewritten as

$$\frac{1}{\hat{V}_1}(v - \hat{v}_{\alpha 1})\hat{v}_{\alpha 1} = -\frac{V_n + \Delta \hat{V}_1}{2}\left[1 + \cos(2\theta_n + 2\Delta\hat{\theta}_1)\right]$$
$$+ \frac{V_n + \Delta V_1}{2}\left[\underbrace{\cos(\Delta\theta_1 - \Delta\hat{\theta}_1)}_{\approx 1} + \cos(2\theta_n + \Delta\theta_1 + \Delta\hat{\theta}_1)\right] \quad (9a)$$

$$\frac{1}{\hat{V}_1}(v - \hat{v}_{\alpha 1})\hat{v}_{\beta 1} = -\frac{V_n + \Delta\hat{V}_1}{2}\sin(2\theta_n + 2\Delta\hat{\theta}_1)$$
$$+ \frac{V_n + \Delta V_1}{2}\left[\sin(2\theta_n + \Delta\theta_1 + \Delta\hat{\theta}_1) - \underbrace{\sin(\Delta\theta_1 - \Delta\hat{\theta}_1)}_{\approx(\Delta\theta_1 - \Delta\hat{\theta}_1) = \Delta\theta_e}\right] \quad (9b)$$

By applying trigonometric identities, (9) can be approximated by (10) at the bottom of the page. Considering (10) and the definitions (3), the governing differential equations of the eSOGI-FLL, which are expressed in (7), can be linearized as

$$\frac{d\Delta\hat{\omega}}{dt} \approx \frac{\lambda}{2}\left[\{1 - \cos(2\theta_n)\}\Delta\theta_e - \frac{1}{V_n}\sin(2\theta_n)\Delta V_e\right]$$
$$+ \frac{\lambda'}{2}\left[\frac{1}{V_n}\{1 + \cos(2\theta_n)\}\Delta V_e - \sin(2\theta_n)\Delta\theta_e\right] \quad (11a)$$

$$\frac{d\Delta\hat{\theta}_1}{dt} \approx \frac{k\omega_n}{2}\left[\{1 - \cos(2\theta_n)\}\Delta\theta_e - \frac{1}{V_n}\sin(2\theta_n)\Delta V_e\right]$$
$$+ \Delta\hat{\omega} + \frac{k'\omega_n}{2}\left[\frac{1}{V_n}\{1 + \cos(2\theta_n)\}\Delta V_e - \sin(2\theta_n)\Delta\theta_e\right] \quad (11b)$$

$$\frac{d\Delta\hat{V}_1}{dt} \approx \frac{k\omega_n}{2}\left[\{1 + \cos(2\theta_n)\}\Delta V_e - V_n\sin(2\theta_n)\Delta\theta_e\right]$$
$$- \frac{k'\omega_n}{2}\left[V_n\{1 - \cos(2\theta_n)\}\Delta\theta_e - \sin(2\theta_n)\Delta V_e\right]. \quad (11c)$$

Using (11), which is a set of LTP differential equations, an LTP model as shown in Fig. 8 can be obtained for the eSOGI-FLL.

C. LTP Modeling of SOGI-FLL

In Section II-A, it was demonstrated that the SOGI-FLL is a special case of the eSOGI-FLL, in which $k' = 0$ and

$\lambda' = 0$. Therefore, the LTP model of the SOGI-FLL can be simply obtained by considering $k' = 0$ and $\lambda' = 0$ in the LTP model of the eSOGI-FLL (Fig. 8). Fig. 9(a) shows the resulting model. The comparison of this model with the basic LTP model of the SOGI-FLL [see Fig. 9(b)], which has been presented in [20], can be informative. The basic LTP model of the SOGI-FLL, contrary to the new one, does not predict the amplitude estimation dynamics. According to Fig. 9(a), there is also a cross-coupling between the amplitude and phase estimation loops of the SOGI-FLL, which the basic LTP model [Fig. 9(b)] neglects it. The reason is that in obtaining the basic LTP model in [20], the grid voltage amplitude variations are neglected.

D. LTP Modeling of EPLL

It has been proven theoretically and numerically in several publications that the EPLL is mathematically equivalent to the SOGI-FLL if $k_p = k_v = k\omega_n$ and $k_i = \lambda$ [7], [12]. Considering this fact, the LTP model of the EPLL can be directly obtained from that of the SOGI-FLL, as shown in Fig. 10(a). The basic LTP model of the EPLL, which has already been presented in [20], may also be observed in Fig. 10(b).

E. LTP Modeling of APF-FLL

It was discussed in Section II-A that the APF-FLL is a special case of the eSOGI-FLL, in which $k' = -k$ and $\lambda' = 0$. Therefore, the LTP model of the APF-FLL can be simply obtained by considering $k' = -k$ and $\lambda' = 0$ in Fig. 8. The resulting model is shown in Fig. 11.

F. LTP Modeling of SSLKF-FLL

We discussed in Section II-A that the SSLKF-FLL is a special case of the eSOGI-FLL, in which $k_\alpha = k\omega_n$, $k_\beta = k'\omega_n$, and $\lambda' = 0$. Consequently, the LTP model of the SSLKF-FLL can be readily obtaining by considering the above relations in Fig. 8. Fig. 12 shows the resultant model.

$$\frac{1}{\hat{V}_1}(v - \hat{v}_{\alpha 1})\hat{v}_{\alpha 1} \approx \frac{1}{2}\left[\overbrace{\Delta V_1 - \Delta\hat{V}_1}^{\Delta V_e} + V_n\cos(2\theta_n)\overbrace{\left\{\cos(\Delta\theta_1 + \Delta\hat{\theta}_1) - \cos(2\Delta\hat{\theta}_1)\right\}}^{\approx 0} - V_n\sin(2\theta_n)\overbrace{\left\{\sin(\Delta\theta_1 + \Delta\hat{\theta}_1) - \sin(2\Delta\hat{\theta}_1)\right\}}^{\approx\Delta\theta_e}\right.$$
$$\left. + \cos(2\theta_n)\underbrace{\left\{\Delta V_1\cos(\Delta\theta_1 + \Delta\hat{\theta}_1) - \Delta\hat{V}_1\cos(2\Delta\hat{\theta}_1)\right\}}_{\approx\Delta V_e} - \sin(2\theta_n)\underbrace{\left\{\Delta V_1\sin(\Delta\theta_1 + \Delta\hat{\theta}_1) - \Delta\hat{V}_1\sin(2\Delta\hat{\theta}_1)\right\}}_{\approx 0}\right]$$
$$\approx \frac{1}{2}\left[\{1 + \cos(2\theta_n)\}\Delta V_e - \{V_n\sin(2\theta_n)\}\Delta\theta_e\right] \quad (10a)$$

$$\frac{1}{\hat{V}_1}(v - \hat{v}_{\alpha 1})\hat{v}_{\beta 1} \approx \frac{1}{2}\left[-V_n\Delta\theta_e + V_n\sin(2\theta_n)\overbrace{\left\{\cos(\Delta\theta_1 + \Delta\hat{\theta}_1) - \cos(2\Delta\hat{\theta}_1)\right\}}^{\approx 0} + V_n\cos(2\theta_n)\overbrace{\left\{\sin(\Delta\theta_1 + \Delta\hat{\theta}_1) - \sin(2\Delta\hat{\theta}_1)\right\}}^{\approx\Delta\theta_e}\right.$$
$$\left. + \sin(2\theta_n)\underbrace{\left\{\Delta V_1\cos(\Delta\theta_1 + \Delta\hat{\theta}_1) - \Delta\hat{V}_1\cos(2\Delta\hat{\theta}_1)\right\}}_{\approx\Delta V_e} + \cos(2\theta_n)\underbrace{\left\{\Delta V_1\sin(\Delta\theta_1 + \Delta\hat{\theta}_1) - \Delta\hat{V}_1\sin(2\Delta\hat{\theta}_1)\right\}}_{\approx 0}\right]$$
$$\approx \frac{1}{2}\left[\sin(2\theta_n)\Delta V_e - V_n\{1 - \cos(2\theta_n)\}\Delta\theta_e\right] \quad (10b)$$
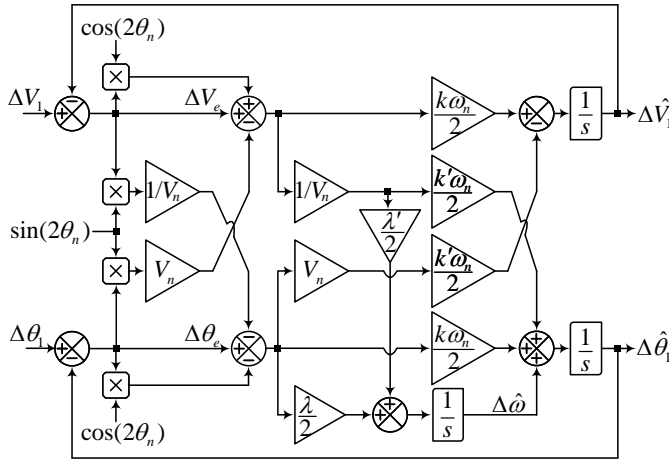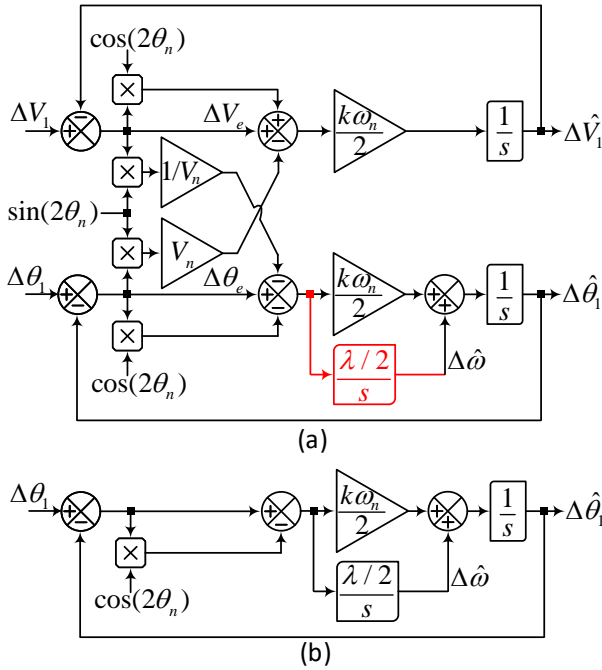
Fig. 8. LTP model of the eSOGI-FLL.

Fig. 9. (a) New LTP model of the SOGI-FLL. (b) Basic LTP model of the SOGI-FLL [20].

G. LTP Modeling of SOGI-FLL-WPF

The SOGI-FLL-WPF, as shown in Fig. 6, is constructed by using a prefilter before the SOGI-FLL input. As we already have an LTP model for the SOGI-FLL [see Fig. 9(a)], the complete LTP model of the SOGI-FLL-WPF can be obtained by modeling the prefilter part and connecting this model with that of the SOGI-FLL.

Modeling of the prefilter of the SOGI-FLL-WPF can be done mathematically by following a similar procedure as that described in Section II-B. However, for the sake of brevity, an intuitive way is presented here. A quick look at Fig. 6 reveals that the prefilter of the SOGI-FLL-WPF is actually a SOGI-FLL without its frequency estimator, which receives an estimation of the grid frequency through a feedback loop. Therefore, the LTP model of this prefilter will be the same as
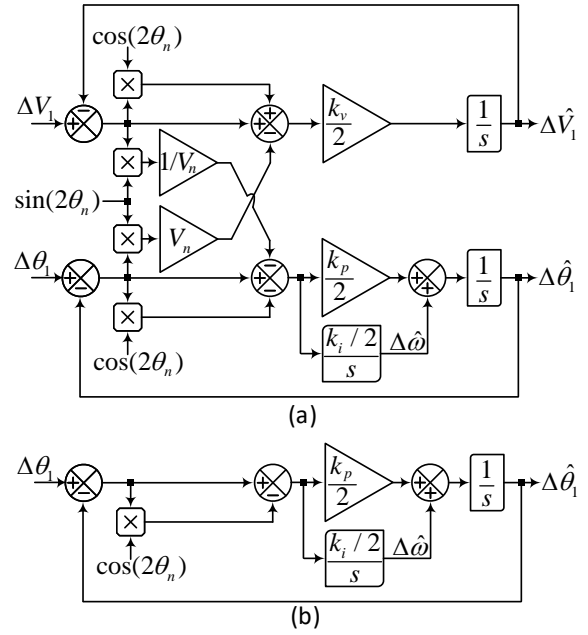

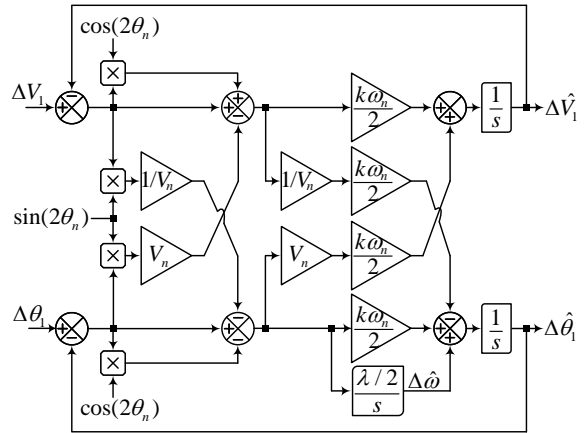Fig. 10. (a) New LTP model of the EPLL. (b) Basic LTP model of the EPLL [20].
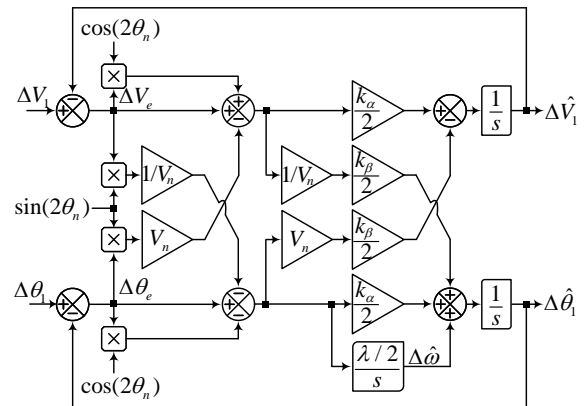

Fig. 11. LTP model of the APF-FLL.

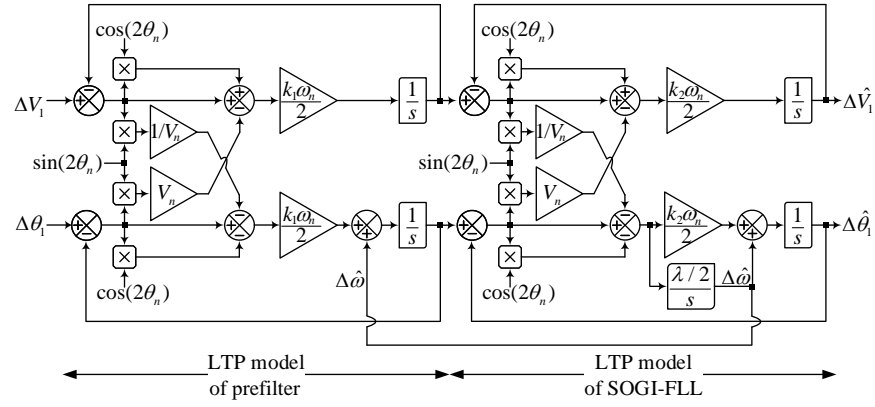Fig. 12. LTP model of the SSLKF-FLL.

Fig. 13. LTP model of the SOGI-FLL-WPF.

TABLE II
CONTROL PARAMETERS

	Parameters
SOGI-FLL [20]	$k = \sqrt{2}$, $\lambda = 49\,384$
EPLL [20]	$k_p = k_v = 444$, $k_i = 49\,384$
APF-FLL	$k = \sqrt{2}$, $\lambda = 49\,384$
SSLKF-FLL [16]	$k_\alpha = 444$, $k_\beta = -141$, $\lambda = 49\,384$
eSOGI-FLL	$k = \sqrt{2}$, $k' = -0.45$, $\lambda = 49\,384$, $\lambda' = 15\,685$
SOGI-FLL-WPF [19]	$k_1 = k_2 = \sqrt{2}$, $\lambda = 23\,948$

Fig. 9(a) but without the highlighted (red color) part. Instead, the signal $\Delta\hat{\omega}$ in the linear model of the prefilter is provided through a feedback loop from the SOGI-FLL model, as shown in Fig. 13.

H. Model Verification

To evaluate the accuracy of the obtained LTP models, the following tests are conducted in Matlab/Simulink.

- Test 1: 10° phase angle jump.
- Test 2: +2 Hz frequency jump.
- Test 3: 0.2 p.u. voltage sag.

In each test, the estimated amplitude $\hat{V}_1$, the estimated angular frequency $\hat{\omega}$, and the phase error signal $\theta_1 - \hat{\theta}_1$ (which is the difference between the actual and estimated phase angles) in each FLL/PLL structure are compared with those predicted by its LTP model. In the case of the SOGI-FLL and EPLL, the results predicted by their basic LTP models [see Fig. 9(b) and Fig. 10(b)] are also shown. Notice that these basic LTP models can only predict the output phase and frequency of the SOGI-FLL and EPLL.

All the FLL/PLL structures under study and their LTP models are discretized with a sampling frequency of 10 kHz. The nominal amplitude and frequency of the signal phase input signal are considered to be 1 p.u. and 50 Hz, respectively. Table I summarizes the selected values for their control parameters.

Fig. 14, 15, and 16 show the model verification results in response to Test 1, 2, and 3, respectively. In all tests, it is observed that the LTP models derived for the SOGI-FLL,

EPLL, APF-FLL, SSLKF-FLL, eSOGI-FLL, and SOGI-FLL-WPF can accurately predict the dynamics of these FLL/PLL structures in the estimation of phase, frequency, and amplitude and also the coupling between these variables. Notice that, in the case of the SOGI-FLL and EPLL, the results predicted by their basic models are also shown. As expected, these models have a lower accuracy compared to the new ones, mainly because they cannot predict the amplitude estimation dynamics and also the coupling between the phase/frequency and amplitude variables.

III. SOGI-FLL ANALYSIS

The main aim of this section is to demonstrate the effectiveness of the LTP models derived in this paper for the stability analysis. For the sake of brevity, this study is only carried out on the SOGI-FLL. As the SOGI-FLL is mathematically equivalent to the EPLL, the results of this study are also valid for the EPLL. The stability analysis of other FLL structures can be performed in a similar manner.

A. Harmonic Transfer Function of SOGI-FLL

From Fig. 9(a), the output signals $\Delta\hat{V}_1$ and $\Delta\hat{\theta}_1$ in the new LTP model of the SOGI-FLL can be expressed in the Laplace domain as

$$\Delta\hat{V}_1(s) = KG(s)\mathcal{L}[(1 + \cos(2\theta_n))\,\Delta V_e(t) - V_n \sin(2\theta_n)\Delta\theta_e(t)] \quad (12a)$$

$$\Delta\hat{\theta}_1(s) = KH(s)\mathcal{L}[(1 - \cos(2\theta_n))\,\Delta\theta_e(t) - \sin(2\theta_n)\Delta V_e(t)/V_n] \quad (12b)$$

where $\mathcal{L}$ denotes the Laplace transform, $\theta_n = 2\omega_n t$, $K = k\omega_n/2$, $H(s) = \frac{s+\Gamma}{s^2}$, $\Gamma = \lambda/(k\omega_n)$, and $G(s) = \frac{1}{s}$.

By replacing the sine and cosine functions in (12) by their equivalent expressions in terms of exponentials, i.e., $\cos(2\theta_n) = \frac{e^{-j2\omega_n t} + e^{j2\omega_n t}}{2}$ and $\sin(2\theta_n) = \frac{je^{-j2\omega_n t} - je^{j2\omega_n t}}{2}$, and considering the frequency shifting property of the Laplace transform, i.e., $\mathcal{L}\left[e^{at}f(t)\right] = F(s - a)$, (12) can be rewritten as (13) at the bottom of the next page. By defining $s_m = s + j(2\omega_n)m$ ($m \in \mathbb{Z}$) and replacing s by s_m in (13), it can be rewritten as (14). In the matrix form, (14) is corresponding to (15). The matrix equation (15) is the open-loop harmonic
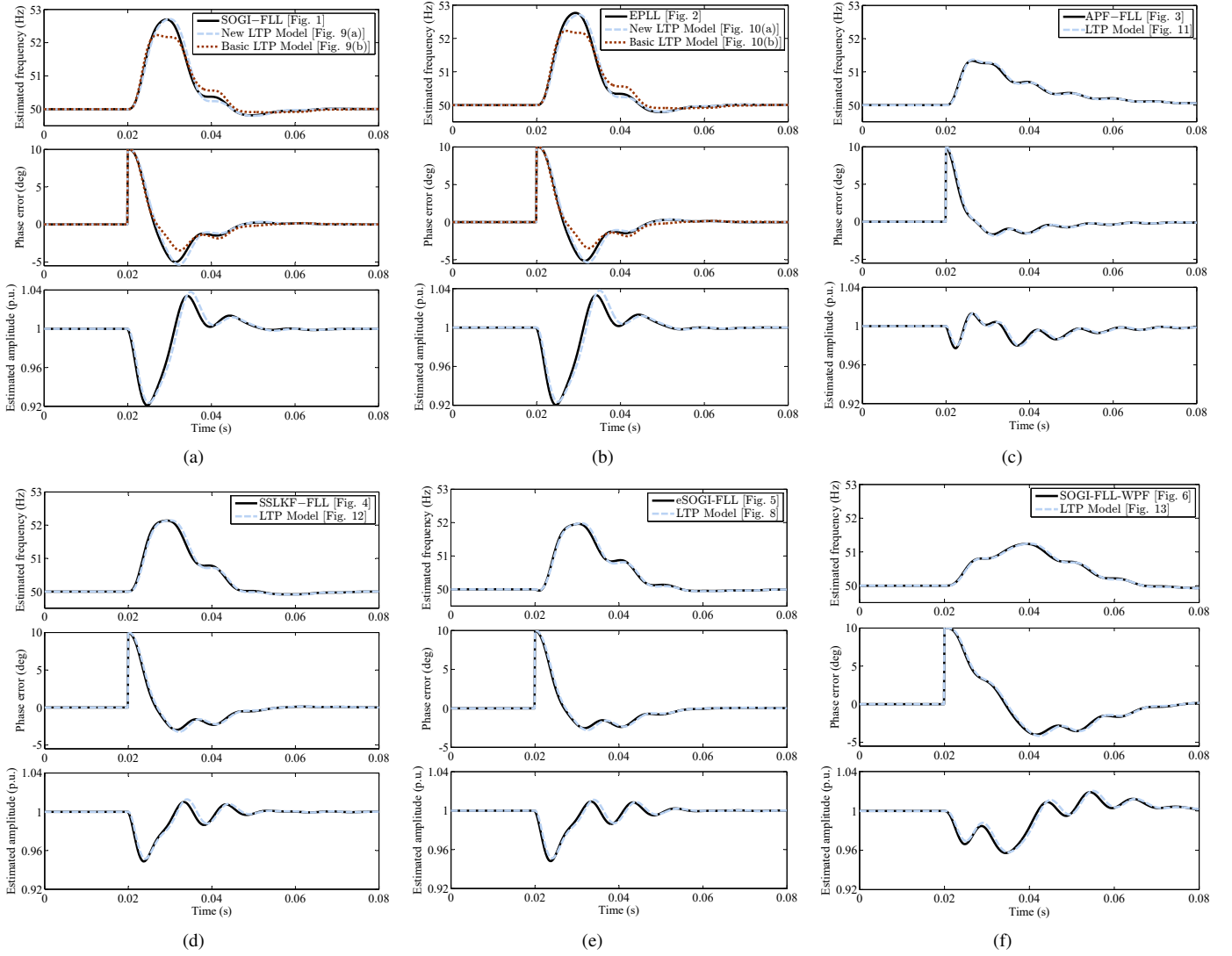
Fig. 14. Model verification in response to Test 1 (10° phase jump). (a) SOGI-FLL. (b) EPLL. (c) APF-FLL. (d) SSLKF-FLL. (e) eSOGI-FLL. (f) SOGI-FLL-WPF.

$$\Delta \hat{V}_1(s) = KG(s)\left[\Delta V_e(s) + \Delta V_e(s - j2\omega_n)/2 + \Delta V_e(s + j2\omega_n)/2 + jV_n\Delta\theta_e(s - j2\omega_n)/2 - jV_n\Delta\theta_e(s + j2\omega_n)/2\right] \tag{13a}$$

$$\Delta \hat{\theta}_1(s) = KH(s)\left[\Delta\theta_e(s) - \Delta\theta_e(s - j2\omega_n)/2 - \Delta\theta_e(s + j2\omega_n)\ /2 + j\Delta V_e(s - j2\omega_n)/(2V_n) - j\Delta V_e(s + j2\omega_n)/(2V_n)\right]. \tag{13b}$$

$$\Delta \hat{V}_1(s_m) = KG(s_m)\left[\Delta V_e(s_m) + \Delta V_e(s_{m-1})\ /2 + \Delta V_e(s_{m+1})/2 + jV_n\Delta\theta_e(s_{m-1})/2 - jV_n\Delta\theta_e(s_{m+1})/2\right] \tag{14a}$$

$$\Delta \hat{\theta}_1(s_m) = KH(s_m)\left[\Delta\theta_e(s_m) - \Delta\theta_e(s_{m-1})/2 - \Delta\theta_e(s_{m+1})/2\ + j\Delta V_e(s_{m-1})/(2V_n) - j\Delta V_e(s_{m+1})/(2V_n)\right]. \tag{14b}$$

$$
\overbrace{\begin{pmatrix} \vdots \\ \Delta\hat{V}_1(s_{-1}) \\ \Delta\hat{\theta}_1(s_{-1}) \\ \Delta\hat{V}_1(s_0) \\ \Delta\hat{\theta}_1(s_0) \\ \Delta\hat{V}_1(s_{+1}) \\ \Delta\hat{\theta}_1(s_{+1}) \\ \vdots \end{pmatrix}}^{\boldsymbol{Y}}
= \overbrace{\frac{K}{\frac{k\omega_n}{2}}}
\overbrace{\begin{pmatrix}
\ddots & \vdots & \vdots & \vdots & \vdots & \vdots & \vdots & \udots \\
\cdots & G(s_{-1}) & 0 & \frac{G(s_{-1})}{2} & -j\frac{V_nG(s_{-1})}{2} & 0 & 0 & \cdots \\
\cdots & 0 & H(s_{-1}) & -j\frac{H(s_{-1})}{2V_n} & -\frac{H(s_{-1})}{2} & 0 & 0 & \cdots \\
\cdots & \frac{G(s_0)}{2} & jV_n\frac{G(s_0)}{2} & G(s_0) & 0 & \frac{G(s_0)}{2} & -jV_n\frac{G(s_0)}{2} & \cdots \\
\cdots & j\frac{H(s_0)}{2V_n} & -\frac{H(s_0)}{2} & 0 & H(s_0) & -j\frac{H(s_0)}{2V_n} & -\frac{H(s_0)}{2} & \cdots \\
\cdots & 0 & 0 & \frac{G(s_{+1})}{2} & jV_n\frac{G(s_{+1})}{2} & G(s_{+1}) & 0 & \cdots \\
\cdots & 0 & 0 & j\frac{H(s_{+1})}{2V_n} & -\frac{H(s_{+1})}{2} & 0 & H(s_{+1}) & \cdots \\
\udots & \vdots & \vdots & \vdots & \vdots & \vdots & \vdots & \ddots
\end{pmatrix}}^{\boldsymbol{\mathcal{F}}(s)}
\overbrace{\begin{pmatrix} \vdots \\ \Delta V_e(s_{-1}) \\ \Delta\theta_e(s_{-1}) \\ \Delta V_e(s_0) \\ \Delta\theta_e(s_0) \\ \Delta V_e(s_{+1}) \\ \Delta\theta_e(s_{+1}) \\ \vdots \end{pmatrix}}^{\boldsymbol{E}}
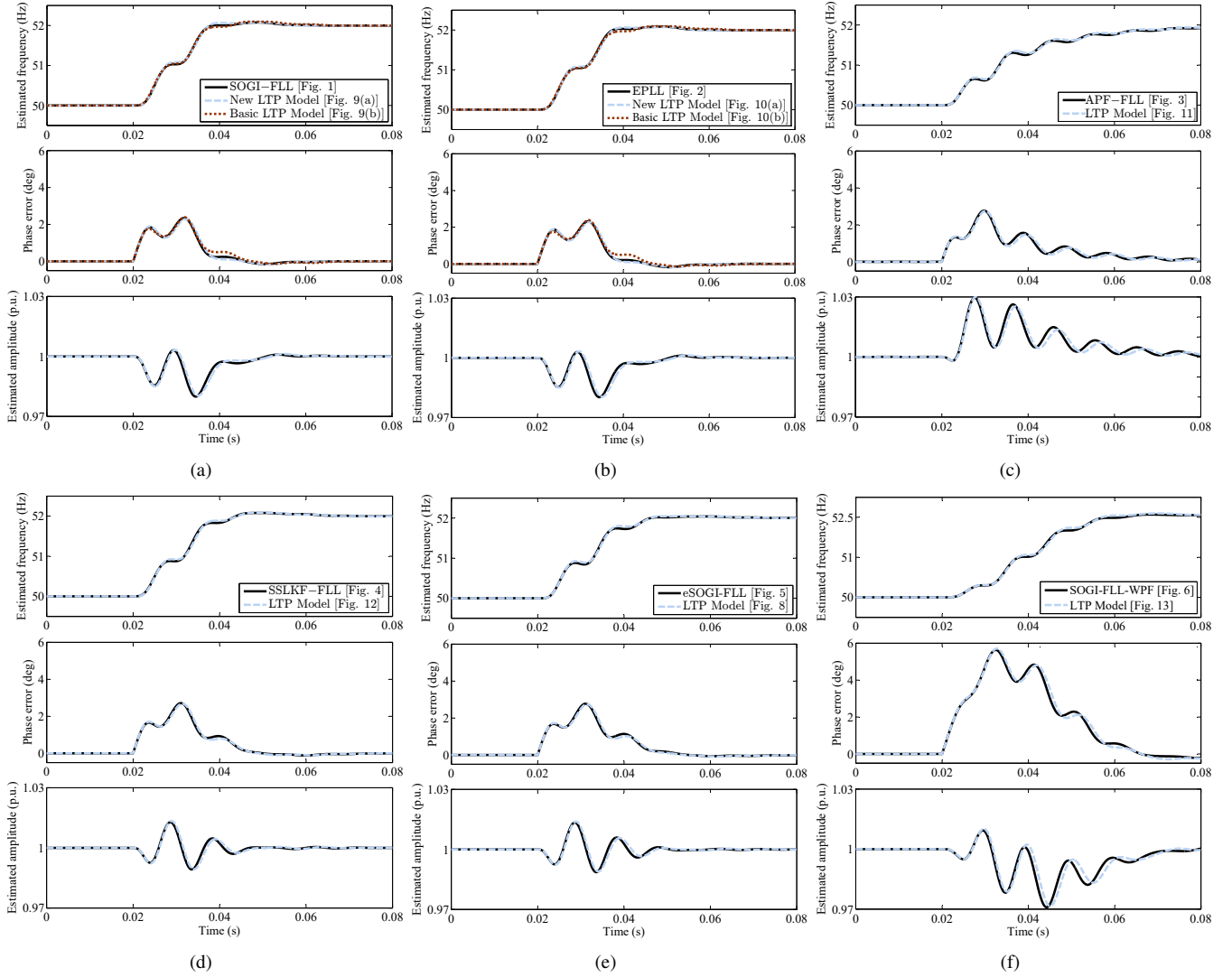\tag{15}
$$

Fig. 15. Model verification in response to Test 2 (+2-Hz frequency jump). (a) SOGI-FLL. (b) EPLL. (c) APF-FLL. (d) SSLKF-FLL. (e) eSOGI-FLL. (f) SOGI-FLL-WPF.

transfer function (HTF) of the SOGI-FLL, which translates its LTP dynamics into an LTI system, as shown in Fig. 17(a). Therefore, the theory of multivariable LTI feedback control is applicable for its analysis. The only point here is that the HTF $\mathcal{F}(s)$ has an infinite dimension. Therefore, its truncated version needs to be considered for the analysis.

B. Overview of Generalized Nyquist Theory for LTP Systems

The generalized Nyquist criterion is a good choice for the SOGI-FLL stability analysis as it is able to determine its stability for a range of control gain (here the control gain K) based on the eigenloci (i.e., the closed curves generated by the eigenvalues) of its open-loop HTF (15). In what follows, the Nyquist criterion for the stability assessment of an LTP feedback control system is briefly explained.

Theorem [21]–[23]: Consider a feedback control system as Fig. 17(a). Assume that $\{\lambda_i(s)\}_{i=-\infty}^{+\infty}$ denote the eigenvalues of the HTF $\mathcal{F}(s)$ for s belonging to a strip defined by $-j\omega_p/2 \leq \mathrm{Im}(s) < j\omega_p/2$ [see Fig. 17(b)]. If we assume that N_p is the number of right-half-side poles of $\mathcal{F}(s)$ in this strip,

then the closed-loop LTP system in Fig. 17(a) is asymptotically stable if and only if the eigenloci of $\mathcal{F}(s)$ encircles the $-1/K$ point exactly N_p times in the counterclockwise direction.

C. Stability Region of SOGI-FLL

Fig. 18 shows the LTP Nyquist plot of the HTF $\mathcal{F}(s)$ in (15) for three different values of Γ: Case a: $\Gamma = 0.2\omega_n = 62.83$, Case b: $\Gamma = \omega_n = 314.16$, and Case c: $\Gamma = 2\omega_n = 628.32$. According to these plots, the following observations can be made.

- Based on the generalized Nyquist theory, the stability in the left, middle, and right Nyquist plots in Fig. 18 is guaranteed if

$$
\begin{aligned}
&\text{Case a } (\Gamma = 0.2\omega_n) &\Rightarrow& \quad -\infty < -\tfrac{1}{K} < -6.398e-4 \\
&\text{Case b } (\Gamma = \omega_n) &\Rightarrow& \quad -\infty < -\tfrac{1}{K} < -3.618e-3 \\
&\text{Case c } (\Gamma = 2\omega_n) &\Rightarrow& \quad -\infty < -\tfrac{1}{K} < -8.707e-3.
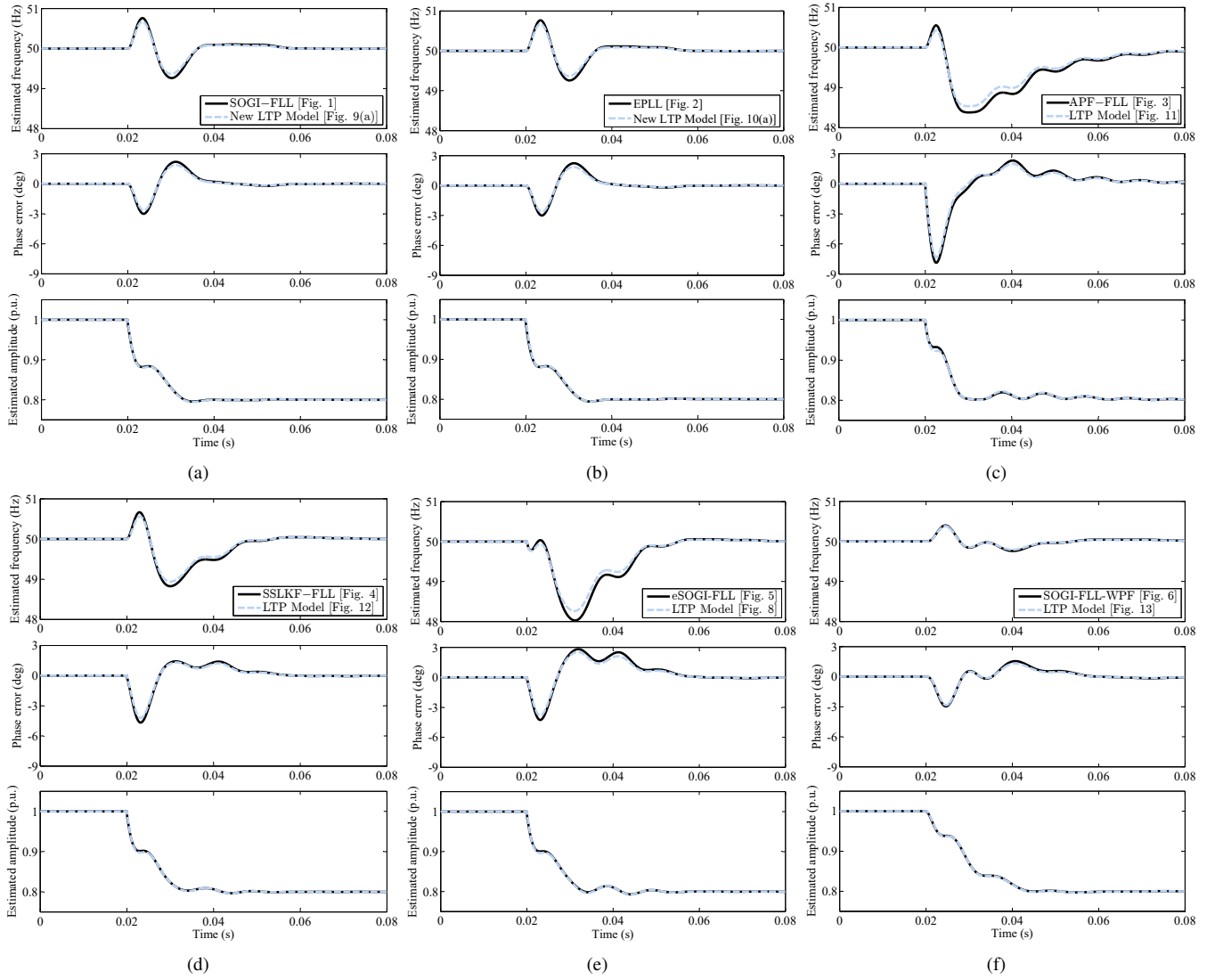\end{aligned}
\tag{16}
$$

Fig. 16. Model verification in response to Test 3 (0.2-p.u. voltage sag). (a) SOGI-FLL. (b) EPLL. (c) APF-FLL. (d) SSLKF-FLL. (e) eSOGI-FLL. (f) SOGI-FLL-WPF.
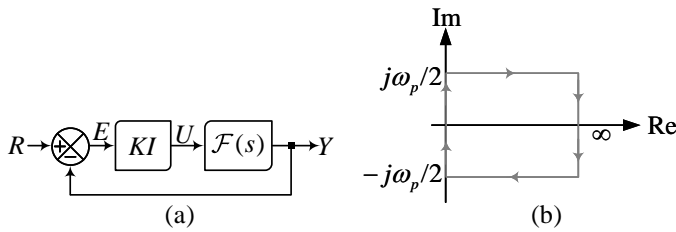

Fig. 17. (a) LTP feedback control system under study. (b) LTP Nyquist contour. I is an identity matrix of the same dimension of the HTF $\mathcal{F}(s)$. All channels have the same gain, i.e., K. For the case of the SOGI-FLL, $\omega_p = 2\omega_n$.

As $K = k\omega_n/2$, where k is the SOGI gain, the above stability regions are corresponding to

$$
\begin{aligned}
&\text{Case a } (\Gamma = 0.2\omega_n) &\Rightarrow& \quad 0 < k < 9.95 \\
&\text{Case b } (\Gamma = \omega_n) &\Rightarrow& \quad 0 < k < 1.76 \\
&\text{Case c } (\Gamma = 2\omega_n) &\Rightarrow& \quad 0 < k < 0.73.
\end{aligned}
\tag{17}
$$

• Increasing the gain Γ reduces the stability range of the

gain k. This fact can be better visualized in Fig. 19, which illustrates the stability range of the gain k versus the gain Γ.

• Even for small values of the gain Γ, the SOGI-FLL may become unstable (see Fig. 19). This observation implies that the stability region of the SOGI-FLL is limiter than what was predicted before using its basic LTP model [Fig. 9(b)]. The reason behind this inaccuracy is that the dynamics of the input signal amplitude have been neglected in obtaining the basic LTP model. Considering these dynamics, as proved in this paper, results in a cross-coupling between the phase and amplitude loops, which explains the rather limited stability region of the SOGI-FLL.

D. dSPACE-based Verification

In section III-C, by applying the generalized Nyquist theory to the open-loop HTF of the SOGI-FLL, its stability region was determined (see Fig. 19). The aim of this section is to
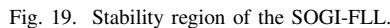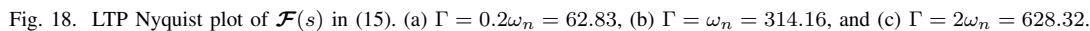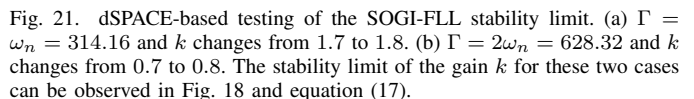
Fig. 18. LTP Nyquist plot of $\mathcal{F}(s)$ in (15). (a) $\Gamma = 0.2\omega_n = 62.83$, (b) $\Gamma = \omega_n = 314.16$, and (c) $\Gamma = 2\omega_n = 628.32$.

Fig. 19. Stability region of the SOGI-FLL.

Fig. 20. Alternative representation of the SOGI-FLL in Fig. 1.

verify the correctness of this region. To this end, Fig. 20, which is an alternative representation of the SOGI-FLL in Fig. 1, is implemented using dSPACE 1006 platform. The sampling frequency, the nominal frequency, and the nominal amplitude are set to 10 kHz, 50 Hz, and 1 p.u., respectively. Two cases are considered: $\Gamma = \omega_n = 314.16$ and $\Gamma = 2\omega_n = 628.32$. According to (17), the stability limits of the gain k for the SOGI-FLL stability in these cases are $0 < k < 1.76$ and $0 < k < 0.73$. In each case, first, the gain k is set to be slightly lower than its upper stability limit. Suddenly, through the control desk of the dSPACE platform, the value of this gain is slightly increased to go a bit beyond its stability limit. This process is highly sensitive to the noise as the SOGI-FLL is very close to its stability border during it. Therefore, to avoid any noise, the single-phase input signal of the SOGI-FLL is generated internally by the dSPACE. The output signals of the SOGI-FLL are then sent out using DAC ports and displayed on a Tektronix digital oscilloscope. To save space, only the estimated frequency by the SOGI-FLL is shown here (see Fig. 21). In both cases, it can be observed that the SOGI-FLL is stable at first and becomes unstable after increasing the control gain k. These results are consistent with theoretical predictions.

Fig. 21. dSPACE-based testing of the SOGI-FLL stability limit. (a) $\Gamma = \omega_n = 314.16$ and k changes from 1.7 to 1.8. (b) $\Gamma = 2\omega_n = 628.32$ and k changes from 0.7 to 0.8. The stability limit of the gain k for these two cases can be observed in Fig. 18 and equation (17).

E. Robustness Metrics

Metrics such as phase margin (PM) and gain margin (GM) demonstrate how close the eigenloci of a feedback control

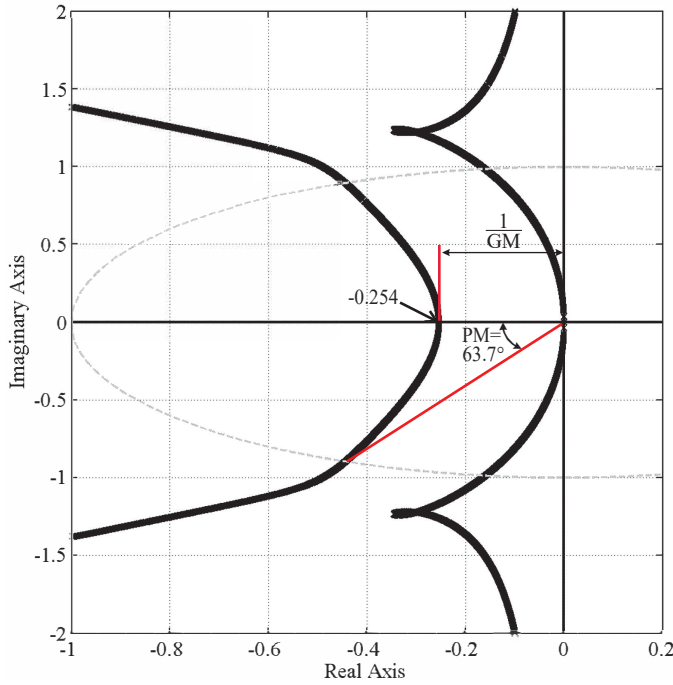Fig. 22. LTP Nyquist plot of the SOGI-FLL open-loop HTF using parameters listed in Table II.
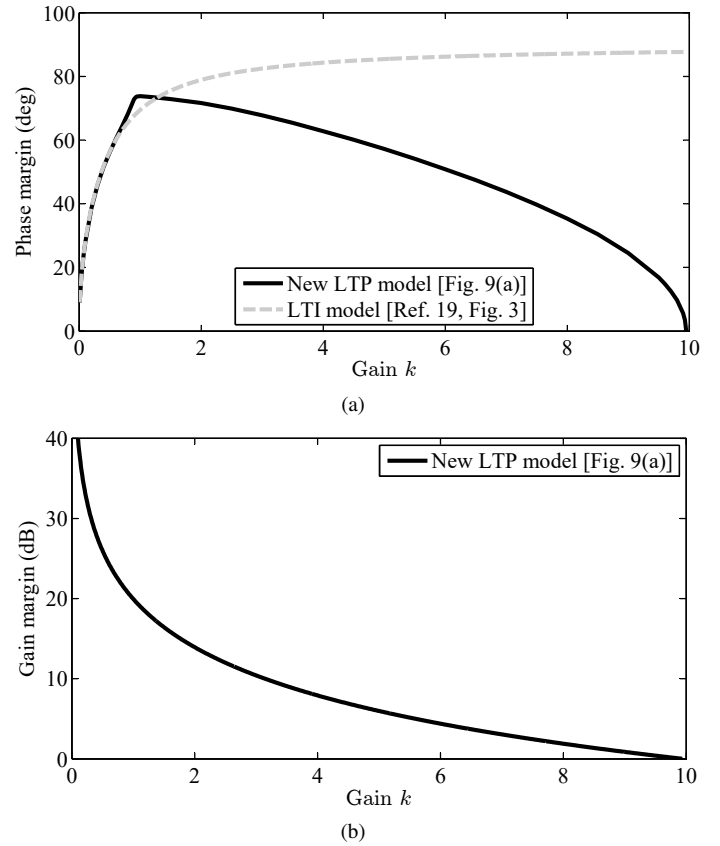

(a)

(b)

Fig. 23. (a) PM and (b) GM of the SOGI-FLL determined using its LTP and LTI models as a function of k. In obtaining these results, $\Gamma = 0.2\omega_n = 62.83$ is considered. According to the equation (17), the stability limit of the gain k for the selected value of Γ is $k_{max} = 9.95$. The GM of the SOGI-FLL according to its LTI model is infinite and, therefore, it cannot be shown.

system is to the critical point $-1 + j0$ and, therefore, provide a measure of the control system robustness. As the HTF translates the LTP system into a multivariable LTI one, the same definitions as those presented for the PM and GM of LTI MIMO feedback control systems are applicable for determining these robustness metrics of an LTP feedback control system. In what follows, the GM and PM in MIMO systems are succinctly defined.

For an LTP feedback control system as Fig. 17(a), the PM is defined as the amount of phase lag that can be added to all branches before the system becomes unstable, and the GM is defined as the minimum gain in dB that can be added to all branches to make the system unstable [24]. Notice that these PM and GM definitions are the same as those in single-input-single-output (SISO) systems. Therefore, they can be determined in a similar manner as a SISO system. To better visualize this fact, Fig. 22 shows the LTP Nyquist plot of the open-loop HTF of the SOGI-FLL. The SOGI-FLL control parameters are the same as those listed in Table II. The PM and GM of the SOGI-FLL in this case, as highlighted in Fig. 22, are equal to $63.7°$ and $GM = 20\log\left(\frac{1}{0.254}\right) = 11.9$ dB.

In this stage, it can be informative to see how increasing the control gains affects the SOGI-FLL stability margins, and to see the difference of the SOGI-FLL LTP and LTI[6] models in determining the stability margins. Fig. 22 shows the variations of the PM and GM of the SOGI-FLL determined using its new LTP model and its LTI model as a function of the gain k. In obtaining these results, $\Gamma = 0.2\omega_n = 62.83$ is selected which, according to (17), results in a stability range of $0 < k < 9.95$ for the control gain k. It can be observed that the LTP

[6]The LTI model of the SOGI-FLL has been presented before in [19] (see Fig. 3 in [19]).

and LTI models are in agreement in determining the PM of the SOGI-FLL as long as the gain k is considerably smaller than its upper stability limit. By further increasing the gain k, the PM determined by the LTP model decreases and finally becomes zero when k reaches its upper stability limit ($k_{max} = 9.95$). On the contrary, the PM determined by the LTI model continues to increase in this condition, which is not consistent with the SOGI-FLL behavior. Regarding the SOGI-FLL GM, it is infinite according to the LTI model and, therefore, it cannot be shown in Fig. 23. However, according to the LTP model, the GM reduces with increasing k and becomes zero when k reaches its upper stability limit. All these observations suggest that the stability margins determined by the LTI model of the SOGI-FLL are trustworthy as long as the control parameters of the SOGI-FLL are far away from its stability/instability border.

F. Discussion

An issue that needs to be discussed here is identifying scenarios where the LTP models derived in this paper may not be very accurate. The LTP modeling of grid synchronization systems, as mentioned in section II-B1, involves defining perturbations around the nominal values of the actual and estimated grid parameters, and the linearization of nonlinear terms around a trajectory. The accuracy of the LTP model
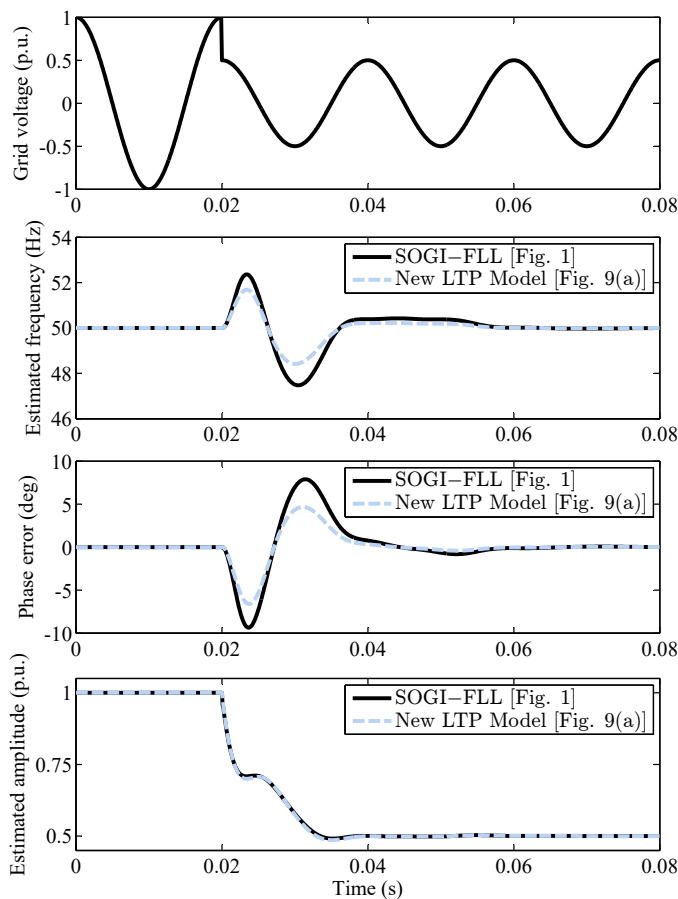
Fig. 24. SOGI-FLL model verification in response to 0.5 p.u. voltage sag. The SOGI-FLL control parameters can be found in Table II.

depends on the size of these perturbations. As long as the perturbations are small, the LTP model provides a good accuracy. For example, as shown in Fig. 14, 15, and 16, the LTP models derived in this paper can provide a remarkable accuracy in response to $10°$ phase jump, $+2$ Hz frequency jump, and $+0.2$ p.u. voltage sag. However, if the magnitude of these disturbances increases, the level of the LTP model accuracy reduces. For example, Fig. 24 shows the results of the SOGI-FLL and its new LTP model in response to a large voltage sag (0.5 p.u. voltage sag). If we compare these results with those shown in Fig. 16(a), a reduction in the accuracy of the SOGI-FLL LTP model is observed.

In summary, the accuracy of the LTP models and, therefore, the accuracy of their predictions reduces in response to large-signal disturbances. It implies that the large-signal modeling should be considered if a high accuracy in response to large disturbances is required.

IV. Conclusion

Developing precise LTP models for the standard single-phase SOGI-FLL and some of its close variants, including the EPLL, APF-FLL, SSLKF-FLL, eSOGI-FLL, and SOGI-FLL-WPF, was the main aim of this paper. To this end, some discussions about the relationship among these grid synchronization systems were conducted. It was mentioned that the EPLL

is mathematically equivalent to the SOGI-FLL under certain conditions. It was also demonstrated that the SOGI-FLL, APF-FLL, and SSLKF-FLL are some special cases of the eSOGI-FLL. Considering these facts, it was concluded that developing a precise LTP model for the eSOGI-FLL suffices for obtaining LTP models for all of the grid synchronization systems under study. The paper was then proceeded with developing an LTP model for the eSOGI-FLL. After some assumptions and definitions and through a step by step mathematical procedure, an LTP model was developed for the eSOGI-FLL. Using this model and considering the relationship among the grid synchronization systems under study, the LTP models of the SOGI-FLL, EPLL, APF-FLL, SSLKF-FLL, and SOGI-FLL-WPF were obtained. The accuracy of all these LTP models was verified numerically using phase/frequency/amplitude jump tests.

To highlight the effectiveness of an LTP model for the analysis of a grid synchronization system, some investigations on the SOGI-FLL and its new LTP model were conducted. It was demonstrated how the open-loop HTF of the SOGI-FLL can be simply obtained using its LTP model. It was shown how using the eigenloci of its open-loop HTF and applying the generalized Nyquist criterion, the stability region of the SOGI-FLL and its robustness metrics (i.e., its PM and GM) can be determined. Finally, the limitation of the SOGI-FLL LTP model was briefly discussed.

The LTP models developed in this paper make two main contributions to the field.

- They facilitate analyzing the SOGI-FLL, EPLL, APF-FLL, SSLKF-FLL, eSOGI-FLL, and SOGI-FLL-WPF as they enable researchers to simply obtain their HTFs and determine their stability region and robustness metrics.
- They pave the way towards the LTP modeling and analysis of advanced single-phase grid synchronization systems, which have been designed based on the SOGI-FLL and its close variants.

References

[1] P. Rodriguez, A. Luna, I. Candela, R. Mujal, R. Teodorescu, and F. Blaabjerg, "Multiresonant frequency-locked loop for grid synchronization of power converters under distorted grid conditions," *IEEE Trans. Ind. Electron.*, vol. 58, no. 1, pp. 127–138, Jan. 2011.

[2] Q. Sun, J. M. Guerrero, T. Jing, J. C. Vasquez, and R. Yang, "An islanding detection method by using frequency positive feedback based on FLL for single-phase microgrid," *IEEE Trans. Smart Grid*, vol. 8, no. 4, pp. 1821–1830, Jul. 2017.

[3] W. Xu, Y. Jiang, C. Mu, and F. Blaabjerg, "Improved nonlinear flux observer-based second-order SOIFO for PMSM sensorless control," *IEEE Trans. Power Electron.*, vol. 34, no. 1, pp. 565–579, Jan. 2019.

[4] M. Mojiri, M. Karimi-Ghartemani, and A. Bakhshai, "Time-domain signal analysis using adaptive notch filter," *IEEE Trans. Signal Process.*, vol. 55, no. 1, pp. 85–93, Jan. 2007.

[5] M. Mansouri, M. Mojiri, M. A. Ghadiri-Modarres, and M. Karimi-Ghartemani, "Estimation of electromechanical oscillations from phasor measurements using second-order generalized integrator," *IEEE Trans. Instrum. Meas.*, vol. 64, no. 4, pp. 943–950, Apr. 2015.

[6] D. Yazdani, M. Mojiri, A. Bakhshai, and G. Joos, "A fast and accurate synchronization technique for extraction of symmetrical components," *IEEE Trans. Power Electron.*, vol. 24, no. 3, pp. 674–684, Mar. 2009.

[7] S. Golestan, J. M. Guerrero, F. Musavi, and J. Vasquez, "Single-phase frequency-locked loops: A comprehensive review," *IEEE Trans. Power Electron.*, vol. 34, no. 12, pp. 11 791–11 812, Dec. 2019.

[8] J. Matas, H. Martin, J. de la Hoz, A. Abusorrah, Y. A. Al-Turki, and M. Al-Hindawi, "A family of gradient descent grid frequency estimators for the SOGI filter," *IEEE Trans. Power Electron.*, vol. 33, no. 7, pp. 5796–5810, Jul. 2018.

[9] C. Yang, J. Wang, X. You, C. Wang, and M. Zhou, "Comparison of discretization methods on the second-order generalized integrator frequency-locked loop," in *2018 IEEE Energy Conversion Congress and Exposition (ECCE)*, Sep. 2018, pp. 3095–3102.

[10] E. Guest and N. Mijatovic, "Discrete-time complex bandpass filters for three-phase converter systems," *IEEE Trans. Ind. Electron.*, vol. 66, no. 6, pp. 4650–4660, Jun. 2019.

[11] G. Escobar, D. d. Puerto-Flores, J. C. Mayo-Maldonado, J. E. Valdez-Resendiz, and O. M. Micheloud-Vernackt, "A discrete-time frequency-locked loop for single-phase grid synchronization under harmonic distortion," *IEEE Trans. Power Electron.*, vol. 35, no. 5, pp. 4647–4657, 2020.

[12] M. Karimi-Ghartemani, "Linear and pseudolinear enhanced phased-locked loop (EPLL) structures," *IEEE Trans. Ind. Electron.*, vol. 61, no. 3, pp. 1464–1474, Mar. 2014.

[13] M. Karimi-Ghartemani, *Enhanced phase-locked loop structures for power and energy applications*. John Wiley & Sons, 2014.

[14] T. Bei and P. Wang, "Robust frequency-locked loop algorithm for grid synchronisation of single-phase applications under distorted grid conditions," *IET Gener. Transm. Distrib.*, vol. 10, no. 11, pp. 2593–2600, 2016.

[15] M. S. Reza, M. Ciobotaru, and V. G. Agelidis, "Accurate estimation of single-phase grid voltage fundamental amplitude and frequency by using a frequency adaptive linear Kalman filter," *IEEE J. Emerging Sel. Top. Power Electron.*, vol. 4, no. 4, pp. 1226–1235, Dec. 2016.

[16] S. Golestan, J. M. Guerrero, J. Vasquez, A. M. Abusorrah, and Y. A. Al-Turki, "Single-phase FLLs based on linear Kalman filter, limit-cycle oscillator, and complex bandpass filter: Analysis and comparison with a standard FLL in grid applications," *IEEE Trans. Power Electron.*, vol. 34, no. 12, pp. 11 774–11 790, Dec. 2019.

[17] C. M. Hackl and M. Landerer, "Modified second-order generalized integrators with modified frequency locked loop for fast harmonics estimation of distorted single-phase signals," *IEEE Trans. Power Electron.*, vol. 35, no. 3, pp. 3298–3309, Mar. 2020.

[18] J. Matas, M. Castilla, J. Miret, L. G. de Vicuna, and R. Guzman, "An adaptive prefiltering method to improve the speed/accuracy tradeoff of voltage sequence detection methods under adverse grid conditions," *IEEE Trans. Ind. Electron.*, vol. 61, no. 5, pp. 2139–2151, May. 2014.

[19] S. Golestan, J. M. Guerrero, J. C. Vasquez, A. M. Abusorrah, and Y. Al-Turki, "Modeling, tuning, and performance comparison of second-order-generalized-integrator-based FLLs," *IEEE Trans. Power Electron.*, vol. 33, no. 12, pp. 10 229–10 239, Dec. 2018.

[20] S. Golestan, J. M. Guerrero, and J. C. Vasquez, "Modeling and stability assessment of single-phase grid synchronization techniques: Linear time-periodic versus linear time-invariant frameworks," *IEEE Trans. Power Electron.*, vol. 34, no. 1, pp. 20–27, Jan. 2019.

[21] S. R. Hall and N. M. Wereley, "Generalized Nyquist stability criterion for linear time periodic systems," in *1990 American Control Conference*, May. 1990, pp. 1518–1525.

[22] N. M. Wereley, "Analysis and control of linear periodically time varying systems," Ph.D. dissertation, Massachusetts Institute of Technology, 1990.

[23] E. Mollerstedt and B. Bernhardsson, "Out of control because of harmonics-an analysis of the harmonic response of an inverter loco-motive," *IEEE Control Systems Magazine*, vol. 20, no. 4, pp. 70–81, Aug. 2000.

[24] A. Emami-Naeini and R. L. Kosut, "The generalized nyquist criterion and robustness margins with applications," in *51st IEEE Conference on Decision and Control (CDC)*, Dec. 2012, pp. 226–231.